Precision Scintillation Distance Measurements

Siqi Liu[1,3]⋆, Ue-Li Pen[1,2]†, J-P Macquart[4]‡, Walter Brisken[5]§, Adam Deller[6]¶

[1] *Canadian Institute for Theoretical Astrophysics, University of Toronto, M5S 3H8 Ontario, Canada*
[2] *Canadian Institute for Advanced Research, Program in Cosmology and Gravitation*
[3] *Department of Astronomy and Astrophysics, University of Toronto, M5S 3H4, Ontario, Canada*
[4] *ICRAR-Curtin University of Technology, Department of Imaging and Applied Physics, GPO Box U1978, Perth, Western Australia 6102, USA*
[5] *National Radio Astronomy Observatory, P.O. Box O, Socorro, NM 87801, USA*
[6] *ASTRON, the Netherlands Institute for Radio Astronomy, Postbus 2, 7990 AA, Dwingeloo, The Netherlands*

12 April 2015

ABSTRACT

We show how interstellar scintillations, combined with VLBI measurements, can be used to measure pulsar distances. Two lensing screens are needed. We apply the technique to archival data on PSR B0834+06. Rough distance estimates, consistent with direct parallax measurements, are obtained. If observations over a six month period had been made at that epoch, we anticipate a 1% distance determination.

With longer ground-based baselines and wider frequency coverage, we speculate that distance determination perhaps as accurate as 0.1% could be possible. This would enable coherent pulsar gravitational wave timing and imaging.

Key words: Pulsar

1 INTRODUCTION

Pulsars have long provided a rich source of astrophysical information due to their compact emission and predictable timing. One of the weakest measurements for most pulsars is their direct geometric distance. For some pulsars, timing parallax or VLBI parallax has resulted in direct distance determinations. For most pulsars, the distance is a major uncertainty for precision timing interpretations, including mass, moment of inertia, and gravitational wave direction(Boyle & Pen 2012).

Direct VLBI observation of PSR B0834+06 shows multiple images lensed by the interstellar plasma. Combining the angular positions and scintillation delays, the authors published the derived effective distance (Brisken et al. 2010) of approximately 1168 ± 23 pc for apexes whose time delays range from 0.1 ms to 0.4 ms, and 1121 ± 59 pc for 1 ms apexes. This represents a precise measurement compared to all other attempts to derive distances to this pulsar. This effective distance is a combination of pulsar-screen and earth-screen distances, and does not allow a separate determination of the individual distances.

A second lensing screen breaks the degeneracy.

⋆ E-mail: sqliu@cita.utoronto.ca
† E-mail: pen@cita.utoronto.ca
‡ E-mail:J.Macquart@curtin.edu.au
§ Email:wbrisken@aoc.nrao.edu
¶ E-mail:deller@astron.nl

2 LENSING

2.1 B0834+06

Our analysis is based on the reduced apex catalog from Brisken et al. (2010). Each identified apex includes a delay, delay rate, RA and dec, one for each of 4 frequency bands, centering 314.5 MHz, 322.5 MHz, 328.5 MHz and 334.5 MHz, all with a bandwidth of 8 MHz. We mapped a total of 9 apexes from the 0.4ms cluster, and 5 from the 1ms cluster, across the 4 frequency bands. This results in an estimate for the mean value, and standard deviation. These are listed in Table 2.4. The time is calculated with $2\tau f/f_D$, which is equivalent to pulsar moving at 640pc plane from the original position to the lensed image position with the velocity calculated. How distance of the pulsar is related to the time delay and how velocity is related to the differential frequency is defined by the following equations:

$$\tau = \frac{D_e \theta^2}{2c},$$

$$f_D = f \cdot \frac{\delta \tau}{dt},$$

where D_e is the effective distance, equivalent to the lens placing at the middle point of the pulsar: $D_e = D_p D_s/(D_p - D_s)$.

A least squares effective distance results in $D_e^M = 1017 \pm 2.8$ for the main 0.4ms cluster and $D_e^S = 1243 \pm 64.1$ for the secondary 1ms cluster. This seems to indicate that the secondary screen is closer to the pulsar. The error bars

are large enough to allow them to be at the same distance, or perhaps a reverse distance ordering. In this paper, we present two analyses for comparison: equidistant, and at the best fit distances. In the first case, no direct distance measurement is possible, but it nevertheless illustrates a robust interpretation of the data.

2.2   Lens Solution

In order to interpret the data, we adopt the lensing model of Pen & Levin (2014). In the absence of a lens model, the fringe rate, delay and angular position cannot be uniquely related. In this model, the lensing is due to projected fold caustics of a thin sheet closely aligned to the line of sight.

Thus, the degeneracy is broken. Furthermore, if we know the distance of the pulsar is 640 pc by parallax, the screen where 0.4 ms scintillation points are deflected, D_s is equal to 392.82 pc. Then with the angle of the axis 25.2 degree west of north, we get the calculated positions. Similarly, for 1 ms pile, the D_s is equal to 422.5 pc and the corresponding calculated positions.

Then we fit a line to this five calculated points. Lying on the fitted line, point 5 share the same $\theta_{\parallel}$ as the point with the largest $\theta_{\parallel}$ in the 0.4 ms pile. Solving the differential frequency f_D of this point, we can calculate the relative velocity of this point to the pulsar, called vA5, which is in the plane that is perpendicular to our line of sight with a direction pointing from point 5 to the position of the pulsar. With the same method, we obtained the $v_{\parallel}$ from the 0.4 ms data. Thus, the total velocity of the pulsar is determined.

That is one lens model fitting. Knowing time delay τ, we can get the distance of the screen; knowing the line and the differential frequency f_D, we can get the velocity of the pulsar.

2.3   Discussion of one lens model

The lens solution appears consistent with the premise of the inclined sheet lensing model(Pen & Levin 2014). The secondary lens only images a subset of the primary lens images. This could happen if the secondary lens screen is just under the critical inclination angle, such that only $3-\sigma$ waves lead to a fold caustic. If the primary lens were at a critical angle, the chance of encountering a somewhat less inclined system is of order unity.

More surprising is the absence of a single deflection image of the pulsar, which is expected at position J. This could happen if the maximum deflection angle is just below critical, such that only rays on the appropriately aligned double deflection can form images. This scenario predicts that at frequencies just below 300 MHz, or a few weeks earlier in time, the pulsar should be seen at position J. We made a plot of the reflected velocity in the direction that is transverse to the first lens plane in Figure 3. From our calculation, it takes 22 days for the injected image of the puslar on the far screen from J to move to the first apex position, and it takes 44 days of the injected image of the pulsar on the far screen from J to move to the fifth apex position.

2.4   Double lens model

However, the distributions of the pile of 1 ms points are not reasonable. According to Fermat's Law, the parallel velocity to the plane should be equal. Thus on the plane which is perpendicular to our line of sight, the injection line should be in agree with the reflection line . If the light of the pulsar are being reflected by one interstellar medium lens, they should be distributed along a line like the axis of the 0.4 ms pile, and we already know that all 1 ms lensed images lie on the magenta line in Figure 2, the only possible position will be J, which is the pedal of the position of the pulsar to the screen line.

Therefore, we consider another model candidate: the double lens model. Respective calculation shows that the light is first refracted by the far screen and then reflected by the near screen.

The first step is to find the positions of the far lens and the near lens. As has been discussed previously, the magenta line is considered to be the far lens, where the positions have a larger effective distance. And the near lens is considered to be the lines that is perpendicular to the 0.4 ms pile axis.

The second step is to find the matched pair of those two lenses. We calculated the $\theta_{\parallel}$ of the respective 1 ms pile observation positions. Here we define the parallel axis to be the axis of the 0.4 ms pile positions. And we got five matched lines, which are marked in Figure 2. They are the second screen lines, where the light got reflected. Those pairs matched the possible pairs of the lens screen. We calculated with the distance of the screen which is calculated in the one lens model, and then move the distance of the far screen little by little to make the calculated time delay match the observation result.

The solved positions in two lens model are plotted in Figure 2.

3   POSSIBLE IMPROVEMENTS

We discuss several strategies which can improve on the solution accuracy. The single biggest improvement would be to monitor over a week, when the pulsar crosses each individual lens, including both lensing systems.

Angular resolution can be improved using longer baselines, for example adding a GMRT-GBT baseline doubles the resolution. Observing at multiple frequencies over a longer period allows for a more precise measurement: when the pulsar is between two lenses, the deflection angle is small, and one expects to see the lensing at higher frequency, where the resolution is higher, and distances between lenses positions can be measured to much higher accuracy.

Holographic techniques(Walker et al. 2008; Pen et al. 2014) may be able to measure delays, fringe rates, and VLBI positions sbstantially more accurately. Combining these techniques, the interstellar lensing could conceivably achieve distance measurements an order of magnitude better than the current published effective distance errors. This could bring most pulsar timing array targets into the coherent timing regime, enabling arc minute localization of gravitational wave sources, lifting any potential source confusion.

Ultimately, the precision of the lensing results would be limited by the fidelity of the lensing model. In the inclined sheet model, the images move along fold caustics. The

f_D(mHz)	σ_{f_D}(mHz)	τ(ms)	σ_τ(ms)	RA(mas)	σ_{RA}(mas)	dec(mas)	σ_{dec}(mas)	time(day)
-12.94	0.19	0.0845	0.0005	2.87	0.11	-8.2	0.09	49.9
-16.8	0.28	0.14125	0.00085	3.86	0.07	-10.6	0.05	64.5
-18.92	0.23	0.188	0.002	5.06	0.2	-10.6	0.13	74.4
-20.4	0.49	0.222	0.003	5.55	0.3	-11.7	0.21	80.8
-21.17	0.61	0.236	0.002	5.12	0.43	-12.6	0.31	83.4
-22.32	0.47	0.2633	0.0003	6.16	0.14	-14.2	0.1	88.0
-24.63	0.4	0.3265	0.0025	6.49	0.29	-14.1	0.2	98.0
-24.94	0.44	0.33775	0.00025	8.29	0.42	-14.4	0.32	99.7
-26.09	0.36	0.37425	0.00063	8.53	0.52	-15.7	0.42	105
-35.06	0.52	0.95	0.002	-15.23	0.69	-21.06	0.7	202
-38.31	0.64	0.976	0.0009	-15.02	0.485	-20.74	0.38	190
-40.17	0.55	1.005	0.0079	-14.14	0.662	-22.27	0.62	187
-41.27	0.54	1.037	0.003	-11.28	0.93	-19.18	1.1	188
-43.08	0.44	1.066	0.005	-8.41	1.7	-24.14	1.4	185

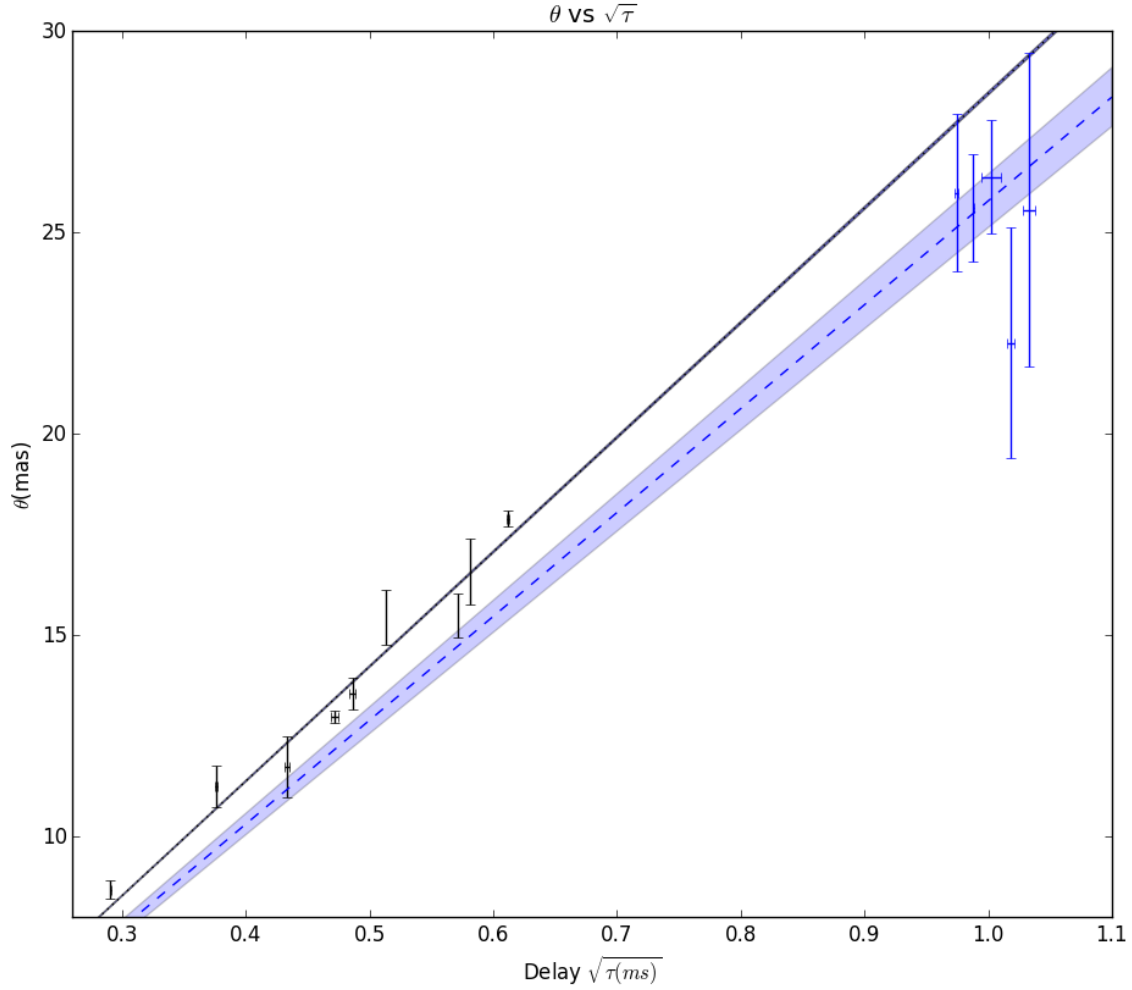**Table 1.** 0.4ms and 1ms observation positions.

Figure 1. θ vs $\sqrt{\tau}$. The black line is the fitted line of the 0.4ms positions, where $k = 28.51$. The blue lines are the fitted lines of the 1ms position, where $k = 25.784$ with an error region of $\sigma_k = 0.66$.
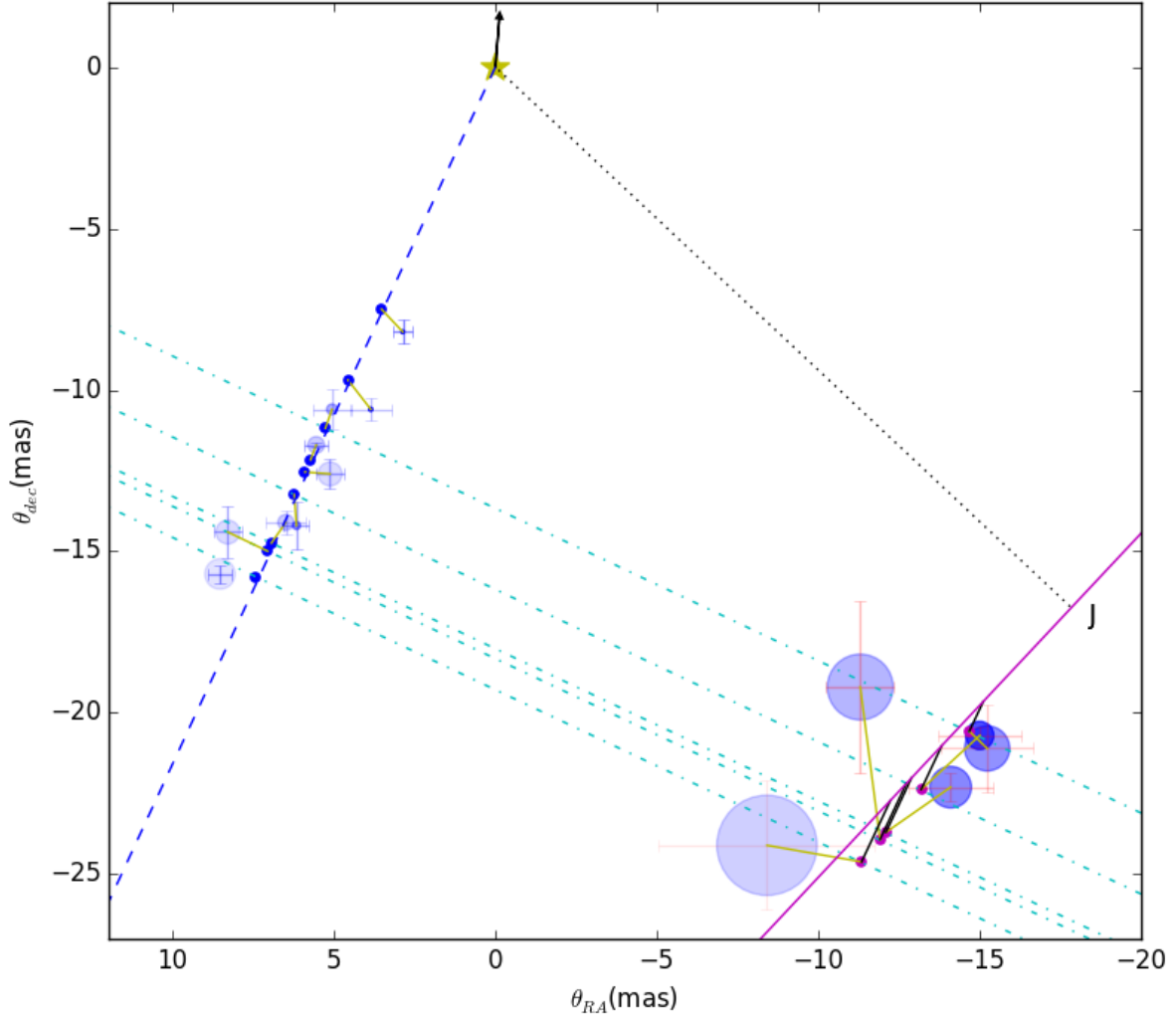
Figure 2. Fitted position of 1ms and 0.4ms data of double lens model and observation data. In both apexes regions, the position of the screen locate at 392.82pc and 425pc. Blue points on the left side are the points that fitted from the f_D and τ of from the 0.4ms observation. Blue line is the fitted line of 0.4ms apex positions, with a 25.2 degree west of the north. The points lie on the left side with errorbars, are the observation points together with their sample errors; while the transparent circles are plotted with population errors, where smaller transparent data are darker. Short solid lines between them are the matched positions of the apexes in $1ms$ region and $0.4ms$ region, which share the same $\theta_\parallel$. The points on the right side are the points that fitted from the f_D and τ of the 1ms observation with an avearage of four bandwidths. Solid line is the fitted line of these positions. Those points with errorbars nearby are the observation points together with their sample errors, while the transparent circles are plotted with population errors. The dotted line on the top right side is vertical to the solid line. Short solid lines connect the observation points and the fitted positions. Middle lines connect the 0.4ms and 1ms fitted positions with the same $\theta_\parallel$. The velocity of the pulsar is 191.4km/s, with a degree 5.56 degree west of north, is also marked out at the top of the figure.
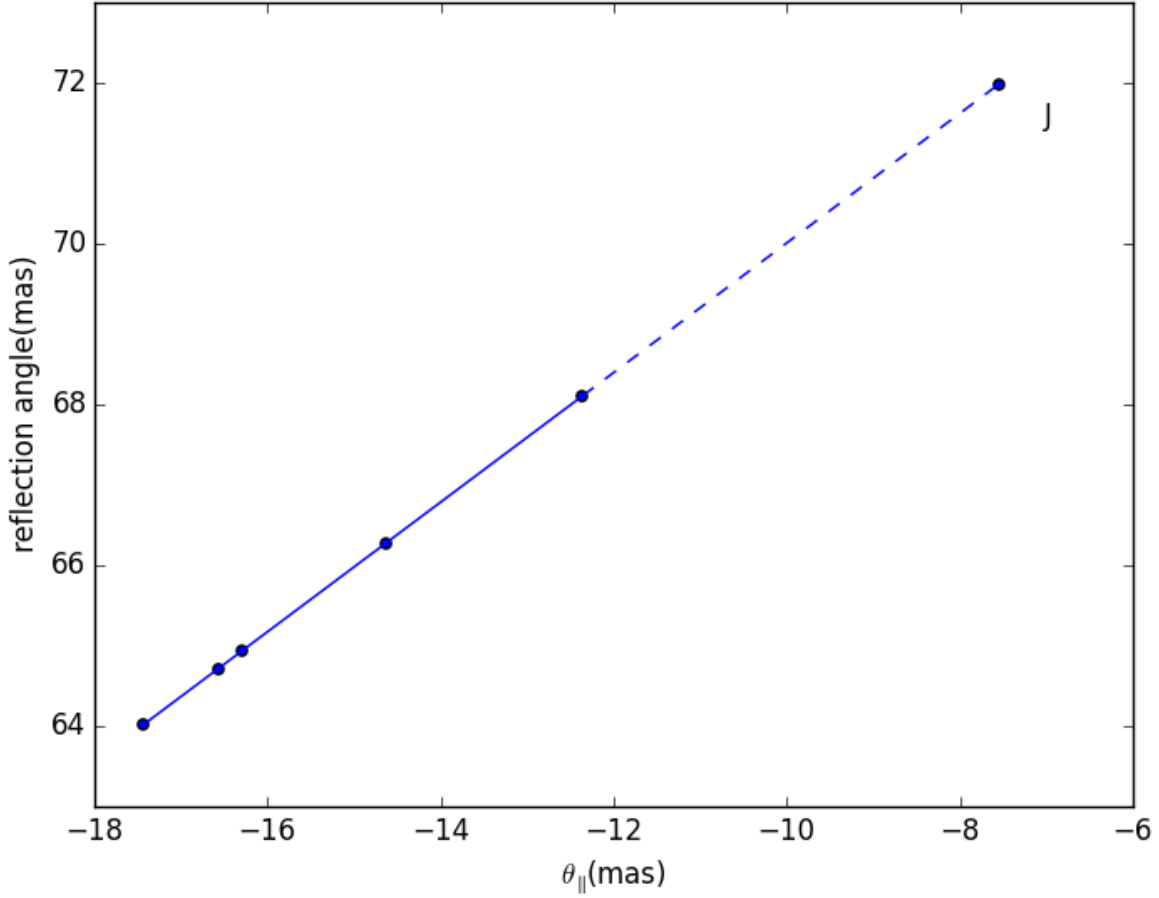
Figure 3. Injection velocity minus reflected velocity over the speed of light. J specifically marked in the paper.

straightness of these caustics depends on the inclination angle, which in turn depends on the amplitude of the surface waves.

4 CONCLUSIONS

We have presented a new technique of two plane interstellar plasma lensing to determine distances to pulsars. We have tested this approach on archival data, showing that in principle solutions can be obtained. We conclude that multi-epoch observations over weeks, at a range of frequencies, might result in much more accurate distance determinations.

5 ACKNOWLEDGEMENTS

REFERENCES

Boyle L., Pen U.-L., 2012, Phys. Rev. D, 86, 124028

Brisken W. F., Macquart J.-P., Gao J. J., Rickett B. J., Coles W. A., Deller A. T., Tingay S. J., West C. J., 2010, ApJ, 708, 232
Pen U.-L., Levin Y., 2014, MNRAS, 442, 3338
Pen U.-L., Macquart J.-P., Deller A. T., Brisken W., 2014, MNRAS, 440, L36
Walker M. A., Koopmans L. V. E., Stinebring D. R., van Straten W., 2008, MNRAS, 388, 1214